20th Australasian Fluid Mechanics Conference
Perth, Australia
5-8 December 2016

Absolute Concentration Measurements of OH* in an Axisymmetric Hydrogen-air Premixed Flame Adjacent to a Hot Graphite Model

M.M. Zhao, R. Choudhury, R. Malpress and D.R. Buttsworth

School of Mechanical and Electrical Engineering
University of Southern Queensland, Toowoomba, Queensland 4350, Australia

Abstract

Absolute concentration of the chemiluminescent radical OH* was determined in an axisymmetric hydrogen-air premixed flame adjacent to a resistively-heated graphite surface. Two-dimensional images of the axisymmetric chemiluminescence from the excited-state of OH were recorded by an ICCD camera with a narrow-band filter at approximately 310 nm. A temperature of around 1800 K was achieved on the graphite surface using an electrical heating power of 5.5 kW. Surface temperatures were measured using a two-color ratio pyrometry (TCRP) technique. The line-of-sight-integrated chemiluminescent emissions that were imaged using the ICCD device were transformed to radial distributions through an Abel inversion method. A new method for calibration of the absolute number density of the radiating radical OH* is proposed based on the intensity ratio of the measured OH* chemiluminescence and the radiation emitted from the hot graphite surface. This is a convenient approach in the present work because adequate signal magnitudes from both these phenomena are acquired by the ICCD device simultaneously during testing.

Introduction

Chemiluminescence refers to the spontaneous light emission from chemically excited species by an electronic exchange process and is a frequently-used diagnostic in combustion research for detecting the location of flame fronts [8] and heat release [6, 10]. The OH* chemiluminescence was recently used as a supersonic combustion diagnostic in [9], and is convenient because the detected radiation is brought about directly by inherent chemical reactions within the oxidation system and the diagnostic avoids the need for expensive and maintenance-prone laser instruments. OH* provides a ready diagnostic for flame and combustion phenomena analysis due to its simplicity and non-intrusive nature.

While there have been numerous experimental investigations and applications of chemiluminescence in flames, most previous research involving the radical's chemiluminescence is limited to qualitative or relative measurements. The measurement of absolute concentration of excited species has been achieved using chemiluminescence measurements with a Raman and Rayleigh scattering calibration by several researchers [11, 14], and [13] appears to be the only published measurements of absolute OH* concentrations in hydrogen/air flames. In H_2/O_2 combustion, the observed self-luminescent emission of UV radiation at a wavelength of around 306 nm is attributed to the OH ($A^2\Sigma^+ - X^2\Pi$) transition from its electronically excited state (typically denoted OH*) to its ground state.

OH* chemiluminescence has been extensively studied [4, 7] and the primary pathways for OH* formation and depletion are commonly proposed as a set of elementary reactions,

$$H + O + M \rightleftharpoons OH^* \qquad (R1)$$

$$OH^* \rightarrow OH + hv \qquad (R2)$$

$$OH^* + M \rightarrow OH + M \qquad (R3)$$

where M is a third body species.

Experimental Arrangement

An external axisymmetric configuration was adopted in an effort to generate high quality data from optical diagnostics that will be suitable for validation of future computational simulations. Combustion experiments where performed in a nominally quiescent test section environment of the free-piston wind tunnel of the University of Southern Queensland – the 'TUSQ' facility, and a detailed description of TUSQ has been reported in [3].

The arrangement of the hot surface axisymmetric model, the fuel delivery system and the optical instruments in the TUSQ facility are illustrated in Figure 1. The fuel supply system can be operated to give either pure hydrogen or premixed hydrogen-air delivery, by the control of two fast-action normally closed solenoid valves (PROCESS SYSTEMS B35). The solenoid valve ① is kept closed if an experiment is conducted with delivery of pure hydrogen fuel.

A K-type fine wire thermocouple (OMEGA, dia. 0.001 inch) with an estimated time constant of 0.01 s and a DRUCK pressure transmitter (PTX1400, 25 Bar) were mounted on the delivery line at a location upstream of the hot model. The mass flow rates of hydrogen and air were measured by an OMEGA flow controller (FMA-2600A) and a ROTA mass meter (YOKOGAWA, RCCS32), respectively. Check valves were mounted in each line to ensure mixing of air and hydrogen does not occur upstream of these devices. Two bespoke flame arresters utilising stainless steel metal mesh with an aperture of 0.132 mm were installed upstream of the check valves. The aperture size of the flame arrestors was chosen based on the quenching distance of about 0.3 mm for stoichiometric hydrogen-air mixtures within the target operation pressures range of 100 to 200 kPa [15]. The flame arresters will prevent flame propagation upstream if the premixed hydrogen-air mixture is ignited accidently and the check valves do not close fast enough. A flexible bag with a volume of approximately 2 liters was utilized as a hydrogen reservoir and was contained in a stainless steel vessel (20 liters approximately).

The hot surface model consisted of a cylindrical graphite tube (dia. 15 mm), a cone with a 9° half angle and other model support components. These were arranged to allow a large amount of electrical power (supplied by a Miller Dynasty 700 welding unit) to be passed through the model during the heating process, generating a large and rapid temperature rise. The water cooling system was designed to remove heat from the metallic sting assembly so that the integrity of soldered joints was maintained during the model heating operation.

Chemiluminescent OH* measurements were recorded using a Princeton Instruments PI-MAX intensified CCD (ICCD) camera mounted above a CaF_2 window on the top side of the test section with an object distance of about 800 mm and an expo-

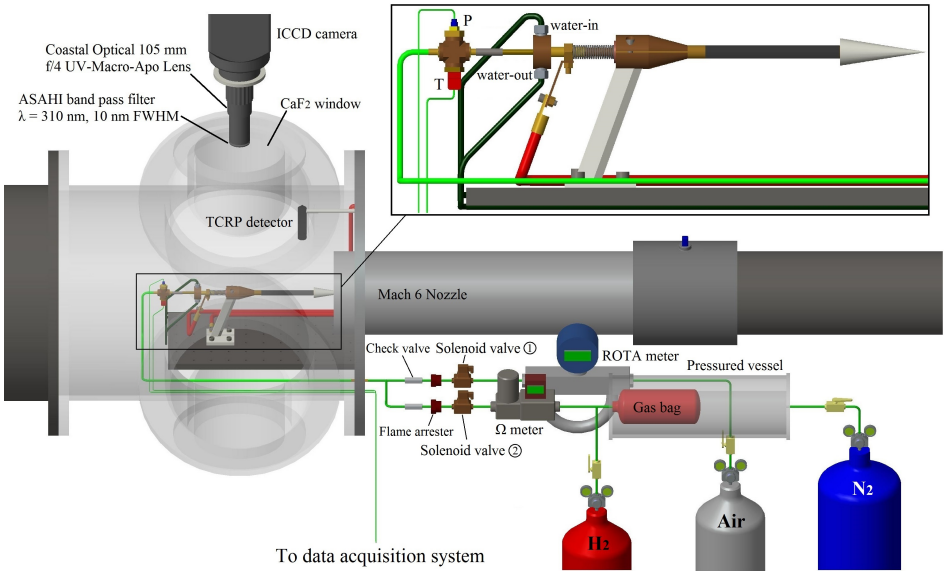

Figure 1: View of hot surface model and instruments arrangement in the TUSQ facility.

sure time of 25 ms. The camera was equipped with an apochromatic, 105 mm focal length UV lens (CoastalOpt 105mm f/4 UV-Macro-Apo) and a narrow-band-pass filter centered at 310 nm with 10 nm FWHM (ASAHI XBPA310) was positioned in front of the lens to capture the radiation emitted in the wavelength range of interest around 308 nm. The resolution of the CCD array used in the camera is 1024×256 px (each pixel $26 \times 26\,\mu$m in size). The sensitivity of the ICCD array was not uniform because of previous damage, so a calibration of the individual pixels relative to an arbitrarily chosen reference point was performed to determine the relative efficiency of each pixel in counts per unit of radiation emitted from a source, as shown in Figure 2.

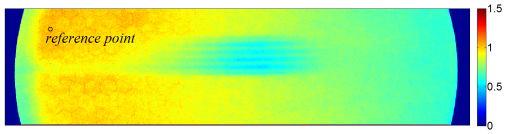

Figure 2: Realtive spatial sensitivity of ICCD pixels.

The two Colour Ratio Pyrometry (TCRP) method used for surface temperature measurement works on the principle that the ratio of any two wavelength intensities emitted by a grey body is unique to a particular temperature and thus the temperature can be determined by the measured ratio of radiation emitted at two wavelengths, without knowledge of the absolute values of radiant intensity or the emissivity. The operating wavelengths can be chosen arbitrarily as long as they are known and significant radiation can be received at these wavelengths for the temperature range of interest. Although graphite does not behave strictly as grey body, the investigation into the wavelength dependent emissivity of graphite has shown a maximum difference of 5 % in the wavelength range of $500 \sim 1000$ nm [1, 12]. For the present study, TCRP with the wavelength ratio of I(850nm)/I(700nm), fast response times (10 kHz) and uncertainties of about ± 50 K was used for time-resolved temperature determination of the heated model during the combustion testing.

Results and Discussion

Figure 3 illustrates the OH* chemiluminescent emission signals in pixel counts from the H_2-air premixed flame. For this figure, the background image that was taken with the flame extinguished as shown in Figure 4 has been subtracted. The conditions of the premixed H_2-air combustion testing are listed in Table 1.

$\dot{m}$ (kg/s)	T_{fuel} (K)	$T_{graphite}$ (K)	$P_{test\ section}$ (kPa)	ϕ
1.40×10^{-4}	320	1798	15	1.03

Table 1: Conditions for the premixed H_2-air combustion testing.

A smoothing process was performed on the image using a 10-pixel moving average filter in order to reduce the noise of the raw OH* chemiluminescence signals, and the smoothed result is shown in Figure 5 for a zoomed-in view. Figure 6 illustrates the raw and smoothed radial signals at $X = 9.2$ mm. The two-dimensional imaged line-of-sight-integrated chemiluminescent emissions recorded by the ICCD camera can be transformed to radial distributions by the inverse Abel transformation. The Abel-inverted results for the smoothed data are plotted in Figure 7. A three-point Abel inversion method based on work by Dasch [5] was used in this case.

The deviation of the transformed results that occurs at the outermost radius (see Figure 7) is caused by the non-zero value and derivative at the outer boundary due to a relatively small view field of ICCD camera. In order to assess the effect of non-zero values at the imaged outer boundary on the Abel-inverted results, the smoothed data was extrapolated to zero based on the second-order polynomial fitting as shown in Figure 6. The results reconstructed from this extrapolation are also plotted in Figure 7. It is clear that the anomalous inverted results at the outer-most radius ($r = 16$ mm) can be corrected using extrapolated data, whereas the peak value and the other values away from the outer-most radius are not affected significantly in the present case. Figure 8 illustrates the radial distribution of the OH* chemiluminescence signals obtained via the 3-points Abel inversion method in the region of interest.

Negative values which are not physically possible appear within

the radial range from 0 to 8.4 mm in Figure 7. For radius values of 7.5 mm or less, the ADU/mm value should be zero theoretically since this radius corresponds with the graphite surface. At least two factors contribute to this error: (1) the hot surface used as a calibrating source for radiation deduction has a slightly different temperature between the backgound image case and the experiment case resulting in a different radiating graphite background intensity; and (2) the slight displacement of the model during the testing made it very difficulty to match the graphite edges perfectly when processing the background radiation deduction. As the Abel inversion is sensitive to the derivative values close to the point being processed, the error at the locations near the graphite edge is amplified. However, the Abel inversion method is effectively marched from r to ∞, the inverted results at locations greater than the graphite edge would not be affected by the graphite edge and background errors.

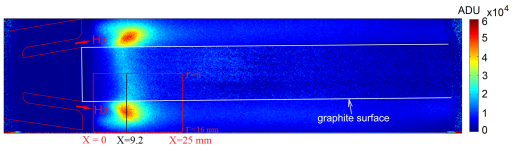

Figure 3: Counts from the ICCD image showing OH* chemiluminescence. The rectangle in red indicates the region of interest for application of the Abel inversion processing. The data along the black line at location of $X = 9.2$ mm is extracted for a more detailed illustration of the Abel inversion analysis.

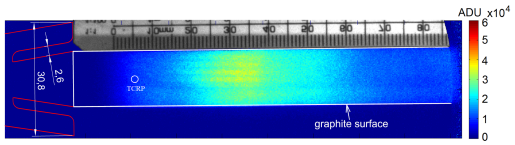

Figure 4: Counts from the ICCD image showing hot surface emission at temperature of 1783 K. The location marked 'TCRP' represents the temperature measurement location (scale: mm).

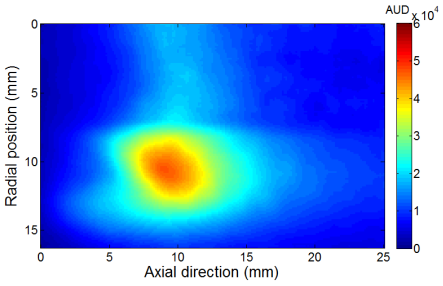

Figure 5: Smoothed OH* chemiluminescence signals in the region of interest.

The absolute number density of the radiating OH* was calculated based on the intensity ratio of the simultaneously measured OH* chemiluminescence and the radiation emitted from the hot graphite surface which is assumed a blackbody. An illustration of the optical detection system is presented in Figure 9. Pixels that collect radiation from ΔA at the intersection of the graphite surface and the axis through its center are chosen as the calibration sources. ΔV represents an observed volume in the path of the line-in-sight integration for a pixel. The ratio of signal intensity S_g (units of ADU) and the Abel inverted

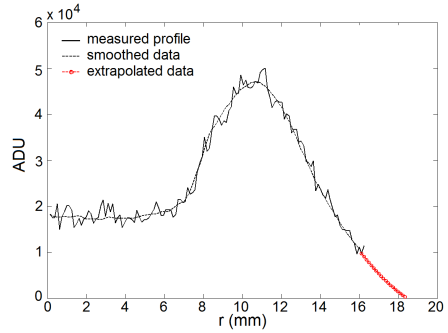

Figure 6: Extracted OH* chemiluminescence signals of pixels at $X = 9.2$ mm from the region of interest.

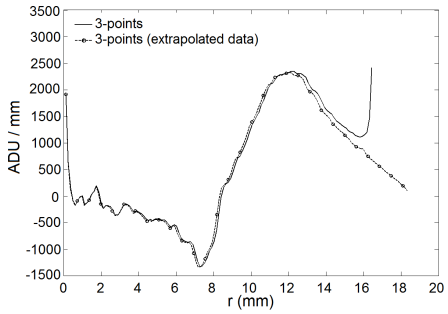

Figure 7: Abel-inverted radial signal distributions at $X = 9.2$ mm.

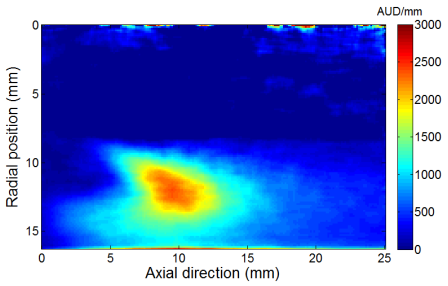

Figure 8: Abel-inverted OH* chemiluminescence signals in the region of interest.

OH* chemiluminescence $S_{OH^*(Abel)}$ (units of ADU/mm) can be related to the number ratio of photons collected by the optical system that are emitted from the hot graphite surface (N_g) and those emitted by excited-state OH* chemiluminescence (N_{OH^*}) within ΔV.

$$\frac{S_g}{S_{OH^*(Abel)}} = \frac{N_g}{N_{OH^*}} = \frac{\int_{\lambda=290}^{330} \frac{I_{b\lambda}}{h\nu}\,\eta\, d\lambda\, \Omega_1\, \xi_1\, \varepsilon\, \Delta t}{\frac{[OH^*]_{em}}{4\pi}\,\eta_{(\lambda=308nm)}\,\Omega_2\,\xi_2\,\varepsilon\,\Delta t}$$
$$= \frac{\int_{\lambda=290}^{330} \frac{E_{b\lambda}}{\pi h\nu}\,\eta\, d\lambda\, \Omega_1\, \xi_1\, \varepsilon\, \Delta t}{\frac{[OH^*]_{em}}{4\pi}\,\eta_{(\lambda=308nm)}\,\Omega_2\,\xi_2\,\varepsilon\,\Delta t} \qquad (1)$$

where $I_{b\lambda}$ W/(m^2 μm sr) and $E_{b\lambda}$ W/(m^2μm) are the monochromatic radiation intensity and emissive power from ΔA into surrounding hemisphere space in which $E_b = \pi I_b$ (Lambert's cosine law), $[OH^*]_{em}$ (N/m^3 $\cdot$ s) is the OH* number density in ΔV that emit photons into surrounding sphere space per second, $h\nu$ is the photon energy, η is the Asahi bandpass filter transmission, Ω is the solid angle over which the light is collected, ξ is the pixel efficiency in counts per photon, ε is the efficiency of the collection optics which is treated as a constant within the nar-

row bandpass range of the optical filter. Δt is the ICCD exposure time. The difference of solid angles Ω_1 and Ω_2 can be neglected since the effective pixel size (0.126×0.126 mm) is very small compared to the object distance (800 mm approximately). The relative sensitivity of the pixels has been determined, see Figure 2. An assumption is made that a constant filter transmission at $\lambda = 308$ nm is applied to OH* emission spectra and this is a reasonable assumption because spectrally resolved measurements of OH* chemiluminescence [2] demonstrate that most of its emission occurs within the wavelength range of 306 nm and 310 nm. Thus the number density of excited-state OH* emitting radiation can be computed.

$$[OH^*]_{em} = \frac{4\, S_{OH^*(Abel)}\, \xi_1}{S_g\, \eta_{(\lambda=308nm)}\, \xi_2} \int_{\lambda=290}^{330} \frac{E_{b\lambda}}{h\nu}\, \eta\, d\lambda \qquad (2)$$

The calculated number density of radiating OH* based on the Abel-inverted radical distributed signals is shown in Figure 10.

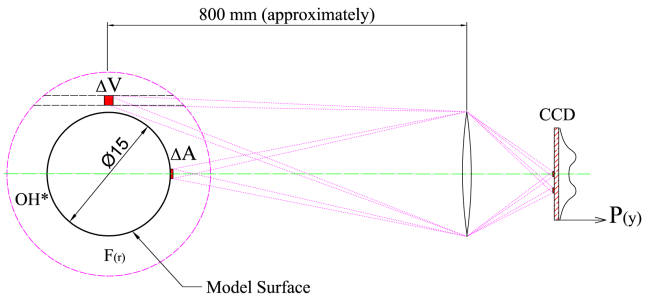

Figure 9: Optical arrangement of OH* chemiluminescence detection system.

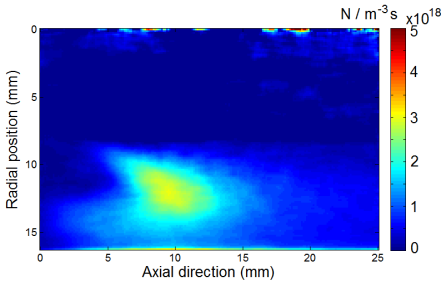

Figure 10: Number density of the radiating OH*.

Conclusions

A number density map of radiating OH* was determined for an axisymmetric hydrogen-air premixed flame based on a calibration method proposed in this paper. For highest quality measurements of axisymmetric chemiluminescence, the following precautions should be observed. (i) An optical configuration with a large depth of field should be used to approximate line-in-sight collection along parallel rays. This can also reduce the 'circle of confusion' effect in which collected light blurs the neighboring pixels. (ii) The radius of the field of view should extend beyond the emissions of interest so that the background level at sufficient radius is acquired.

References

[1] Balat-Pichelin, M., Robert, J. and Sans, J., Emissivity measurements on carbon–carbon composites at high temperature under high vacuum, *Appl. Surf. Sci.*, **253**, 2006, 778–783.

[2] Brieschenk, S., Lorrain, P., Capra, B., Boyce, R., McIntyre, T. J., Kleine, H. and O'Byrne, S., Chemiluminescence imaging in supersonic combustors operating in radical-farming mode, in *18th AIAA/3AF International Space Planes and Hypersonic Systems and Technologies Conference, Tours, France, AIAA 2012-5854*, 2012.

[3] Buttsworth, D. R., Ludwieg tunnel facility with free piston compression heating for supersonic and hypersonic testing, in *Proceedings of the 9th Australian Space Science Conference*, National Space Society of Australia Ltd., 2010, 153–162, 153–162.

[4] Carrington, T., Electronic quenching of OH (2Σ+)in flames and its significance in the interpretation of rotational relaxation, *The Journal of Chemical Physics*, **30**, 1959, 1087–1095.

[5] Dasch, C. J., One-dimensional tomography: a comparison of abel, onion-peeling, and filtered backprojection methods, *Appl. Opt.*, **31**, 1992, 1146–1152.

[6] Hall, J. M. and Petersen, E. L., An optimized kinetics model for oh chemiluminescence at high temperatures and atmospheric pressures, *Int. J. Chem. Kinet.*, **38**, 2006, 714–724.

[7] Kathrotia, T., Fikri, M., Bozkurt, M., Hartmann, M., Riedel, U. and Schulz, C., Study of the H+ O+ M reaction forming OH*: Kinetics of OH* chemiluminescence in hydrogen combustion systems, *Combust. Flame*, **157**, 2010, 1261–1273.

[8] Kojima, J., Ikeda, Y. and Nakajima, T., Basic aspects of OH(A), CH(A), and C2(d) chemiluminescence in the reaction zone of laminar methane–air premixed flames, *Combust. Flame*, **140**, 2005, 34–45.

[9] Laurence, S. J., Schramm, J. M., Karl, S. and Hannemann, K., An experimental investigation of steady and unsteady combustion phenomena in the hyshot ii combustor, *AIAA Journal 2011-2310*.

[10] Najm, H. N., Paul, P. H., Mueller, C. J. and Wyckoff, P. S., On the adequacy of certain experimental observables as measurements of flame burning rate, *Combust. Flame*, **113**, 1998, 312–332.

[11] Nau, P., Krüger, J., Lackner, A., Letzgus, M. and Brockhinke, A., On the quantification of OH*, CH*, and C2* chemiluminescence in flames, *Appl. Phys. B*, **107**, 2012, 551–559.

[12] Neuer, G. and Jaroma-Weiland, G., Spectral and total emissivity of high-temperature materials, *Int. J. Thermophys.*, **19**, 1998, 917–929.

[13] Smith, G. P., Luque, J., Park, C., Jeffries, J. B. and Crosley, D. R., Low pressure flame determinations of rate constants for OH(A) and CH(A) chemiluminescence, *Combust. Flame*, **131**, 2002, 59–69.

[14] Walsh, K., Long, M., Tanoff, M. and Smooke, M., Experimental and computational study of CH, CH*, and OH* in an axisymmetric laminar diffusion flame, in *Symposium (International) on Combustion*, Elsevier, 1998, volume 27, 615–623, 615–623.

[15] Yang, S., Chung, S. and Kim, H., Effect of pressure on effectiveness of quenching meshes in transmitting hydrogen combustion, *Nucl. Eng. Des.*, **224**, 2003, 199–206.